Foam Drainage: Experiments and a New Model

Stephan A. Koehler, Sascha Hilgenfeldt, Howard A. Stone
Pierce Hall, Division of Engineering & Applied Sciences
Harvard University, Cambridge MA, USA

1 Abstract

We present a new experimental method for determining the spatial and temporal variations of the liquid volume fraction distribution in aqueous foams. We use this method to study forced drainage through a soap foam, where a constant liquid flux at the top of a vertical column filled with dry foam produces a downwards traveling wave with a constant velocity and uniform liquid content. These experiments show power-law behaviors that are inconsistent with existing foam drainage models. We generalize the foam drainage equation and propose a zero-stress boundary condition on the liquid flow which yields results in good agreement with the experiments.

2 Introduction

In everyday life we continually come in contact with foams [1, 2], from washing dishes to foods to the seat cushions on which we sit. Recently there has also been interest in foaming metals to make porous ultra-light metallic foams, which are useful in certain mechanical applications [3, 4]. Many foams are made by introducing bubbles into a liquid, and an important control issue is the liquid flow and uniformity of the liquid distribution. It is unclear how the dynamics of fluid flow vary for different kinds of foams, or how the boundary conditions at the liquid/gas interface are determined. Even the fluid dynamics of aqueous foams, which perhaps are the simplest and easiest system to study, are poorly understood [5, 6, 7]. Here we report new experimental results for drainage of aqueous foams along with a new model which captures the most robust features of the experiments.

Foam drainage is the flow of liquid through the interstitial spaces between the bubbles, and is resisted by viscous damping and driven by capillarity and usually gravity [1, 2, 8, 9, 10]. However in microgravity, capillarity is the only driving force of the flow. It is convenient to idealize a foam as a collection of regular tetrakaidecahedral bubbles with edge length L (see Fig. 1a) [11]. Channels are the regions between three touching bubbles, and nodes are the regions between four touching bubbles (see Fig. 1b). On the scale of single bubbles the flow is very complicated: liquid moves through channels from node to node where the flow merges, mixes and splits. Also the liquid/air interface flows in some complicated fashion along the channels. However on a macroscopic scale simple ordered flow is often observed and it is possible to successfully describe foam drainage using simple models.

2.1 Foam Geometry

Surface tension acts to minimize the surface area of the bubbles in (quasi-)equilibrium, and results in a constant curvature, apart from the faces. The surfaces of the bubbles of aqueous foams are coated with surfactants which are necessary to stabilize the faces against rupture by providing a disjoining force that keeps opposing faces from merging. Fig. 1b shows the shape of a typical network unit computed using the Surface Evolver [12] which minimizes the surface energy for a given liquid volume. Here the contact angle where the two channel walls meet at the face is zero, and the liquid content of the face is zero. The amount of interstitial liquid is related to the curvature, so as the curvature decreases the edges and corners of the polygonal bubbles become rounder and the volume fraction of liquid, ϵ, increases.

D. Weaire and J. Banhart: *Foams and Films*, © MIT Verlag Bremen (1999)

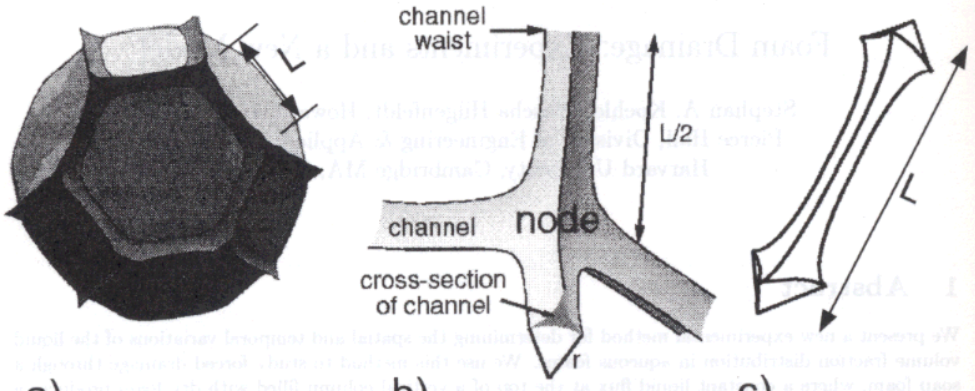

Figure 1: The (idealized) Kelvin foam is composed of tetrakaidecahedra as in a) with edge length L (reproduced from a figure by A. Kraynik, private communication). A liquid network unit composed of one node and four half-channels with corresponding volume fraction $\epsilon = 0.005$ is shown in b) which has been generated using the Surface Evolver [12]. A "dog-bone" shaped liquid network unit with one channel and two quarter-nodes at each end is sketched in c).

Fig. 2 shows a plot of ϵ vs the characteristic radius of curvature $r = (r_1^{-1} + r_2^{-1})^{-1}$ with r_1 and r_2 being the principal radii of curvature. The points are computed for the idealized tetrakaidecahedral foam using the Surface Evolver, and the solid line is a curve fit

$$\epsilon = \delta_\epsilon \left(\frac{r}{L}\right)^2 + \delta' \left(\frac{r}{L}\right)^3 \quad \text{where } \delta_\epsilon = 0.171\,, \delta' = 0.20 \tag{1}$$

to these points. Since we are dealing with dry foams, $r \ll L$, and the approximation

$$r \approx L\sqrt{\frac{\epsilon}{\delta_\epsilon}} \tag{2}$$

is good for volume fractions $\epsilon \lesssim 0.1$. A simple geometrical argument for this polynomial fit (1) can be made as follows.

Foams with low liquid content ($\epsilon \lesssim 0.05$) have channels that are long and slender and contain more liquid than the nodes. With decreasing ϵ the transverse radius of curvature approaches r from above because the longitudinal radius of curvature becomes very large. The cross-sectional area of a channel is $(\sqrt{3} - \pi/2)r^2$, which is the area between three contiguous circles of radius r, and the channel length approaches L. Neglecting small overlap regions in the junctions, the liquid content of a tetrakaidecahedral bubble is $12(\sqrt{3} - \pi/2)r^2 L$ because there are twelve complete channels per bubble. The volume of the tetrakaidechedron is $2^{7/2}L^3$, so the liquid volume fraction due to the channels is $12(\sqrt{3}-\pi/2)2^{-7/2}(r/L)^2$, which is the first term on the right-hand side of (1). For foams with low liquid content, the channels account for almost all the liquid, and we will neglect the higher-order corrections. These corrections arise from the presence of nodes which (i) diminish the length of the channels by $\mathcal{O}(r)$, and (ii) introduce a node volume $\mathcal{V}_n = \delta_n r^3$. This leads to the δ' term from (1), the only genuine fit parameter in the equation.

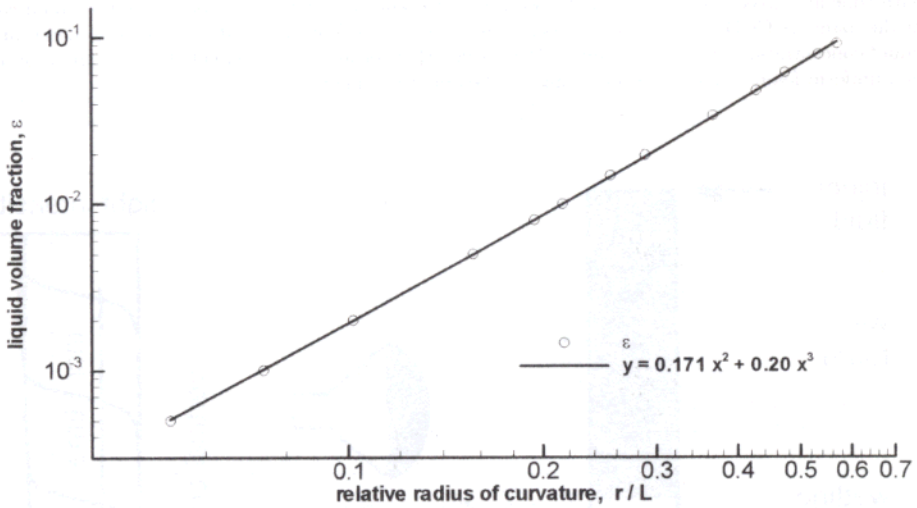

Figure 2: Liquid volume fraction, ϵ, of the idealized Kelvin foam versus r/L as computed by the Surface Evolver [12]. The solid line shows good agreement with a simple polynomial (see (1)).

2.2 Foam As a Porous Medium

It is useful to make an analogy between the drainage of a foam to the flow of liquid through a porous medium such as sand or a packed bed of spheres [13, 14]. The pore density and dimensions determine the permeability of the porous medium to liquid flow. Darcy's law relates the permeability k of a porous medium to the average liquid velocity through the interstitial space, $\mathbf{v}$, and the driving pressure gradient, $\mathbf{G}$,

$$\mathbf{G} = \mu \mathbf{v}/k \tag{3}$$

where μ is the viscosity of the interstitial liquid. Permeability has dimensions of length^2, and scales with the square of a characteristic pore size. For foams the interstitial space plays the role of the pores through which liquid can pass. Unlike conventional porous media, the interstitial space of a foam is not fixed and can easily be changed because the bubbles are deformed as liquid passes through and this modifies the permeability.

There is a considerable body of literature devoted to the drainage of liquid through aqueous foams ([1, 2, 8, 9, 16]). The standard model of foam drainage is based upon a Poiseuille-type flow through the channels with a no-slip boundary condition at the liquid-air interface, thereby treating the foam as a porous medium with changing pore size. However predictions from this model disagree with our experimental results as will be described below.

3 Experimental Procedure

To study foam drainage we have developed a new measurement scheme. The experiment consists of a vertical *foaming tube* that is long and narrow (approximate dimensions of 1.5 m by 2.5 cm). This tube is filled with a soap solution at the bottom, and a very slow flow of gas (air or C_2F_6) produces a constant supply of bubbles at a rate of about 0.4 mm/sec. The solution is composed of tap water, Dawn dish-washing detergent and dissolved fluorescein salt in the ratio of 1:0.025:0.0025 by weight. Glass frits were

used to generate the bubbles, except for the largest bubbles which were made with a capillary tube. The foaming tube is filled with a foam containing very little liquid, less than 0.01% by volume, which we refer to as a *dry* foam. As the foam is constantly being replenished from the bottom, it does not age or coarsen with time at a fixed position. UV lights excite fluorescence in the foam, according to the liquid content of the foam. A CCD digital camera records the fluorescence from which it is possible to determine the liquid concentration profile of the foam. We verified that for low liquid content the fluorescence intensity of a uniform foam is linearly proportional to the liquid volume fraction.

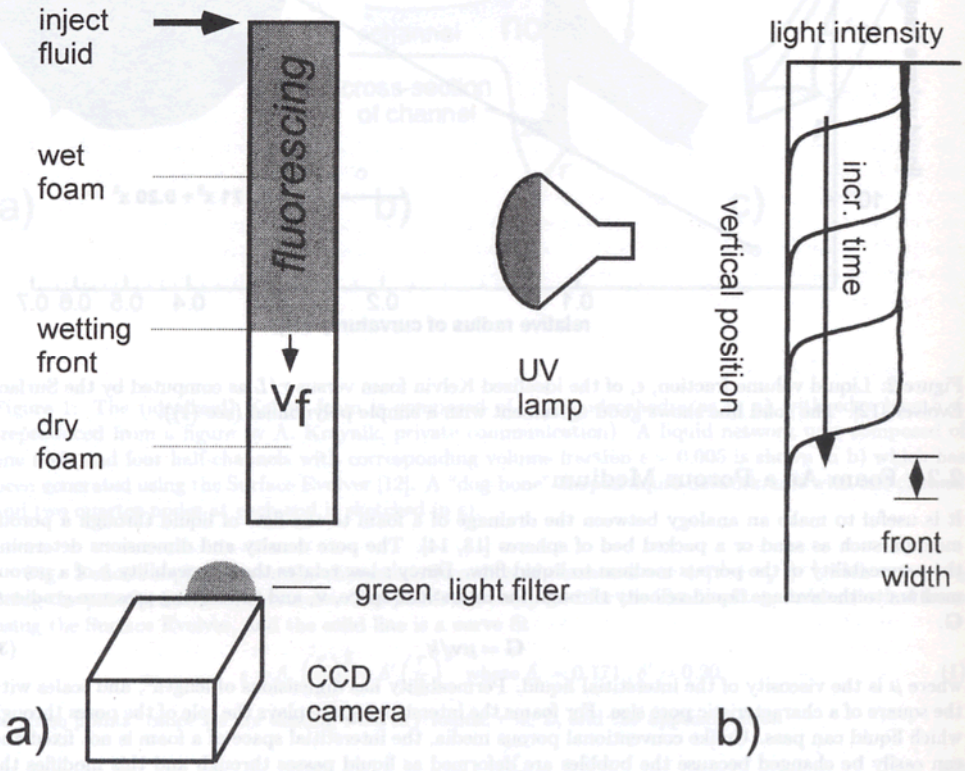

Figure 3: a) The forced drainage experiment consists of a camera that records the fluorescence of the foam illuminated by UV light. The forced drainage wave maintains its profile as it moves downwards through the foam with constant velocity v_f. Fluorescence profiles of the drainage wave are shown for four successive times in b).

Fig. 3a shows a schematic of the *forced drainage* experiment. A constant flux of the solution is added at the top of the foaming tube, which initially is filled with dry foam. The liquid drains down the foam with a downwards moving front at a constant velocity that separates the remaining dry foam below from the growing wet region above. The intensity profiles at four successive times in Fig. 3b show the drainage wave making its way down the foam tube. Behind the front the fluorescing intensity, and thus the liquid content is constant. We record the front velocity, v_f, as a function of the draining flux, Φ, of liquid through the foaming tube. Because the foam is being generated at the bottom at a constant rate it is necessary to add the rate at which it rises to the downwards front velocity of the drainage wave.

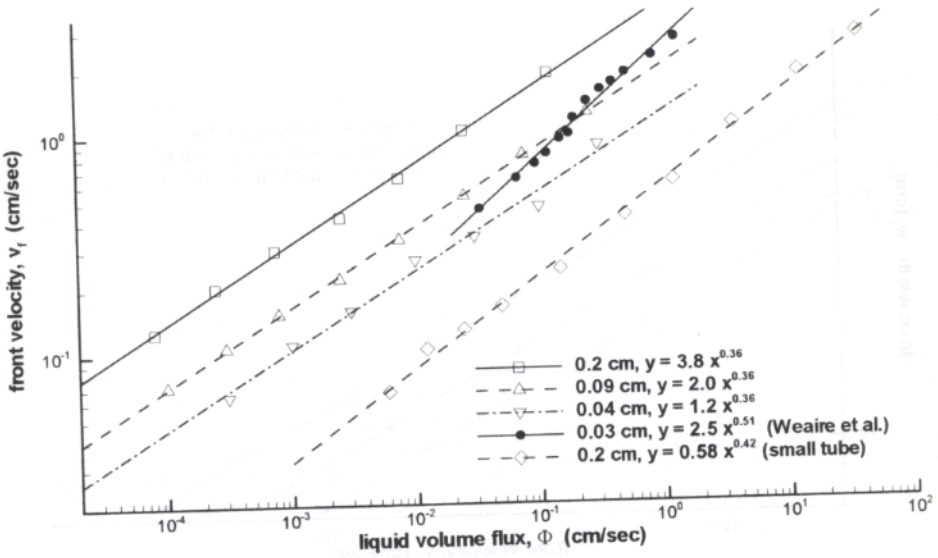

Figure 4: Forced drainage results show the power-law behavior of v_f vs Φ. The top three curves show that $v_f \propto \Phi^{0.36}$ and that v_f increases with increasing bubble size L. The solid circles are data taken from [15], and the bottom curve shows the effect on the front velocity of the walls when the bubble size is comparable to the tube diameter.

4 Experimental Results

Fig. 4 shows the measured relationship between the front velocity, v_f, and the flux, Φ, of the forced drainage experiment. There is a family of three curves corresponding to three different bubble sizes, characterized by an edge length L. Faster drainage rates are found for larger bubbles. Remarkably there is a definite power-law behavior which spans more than three decades of Φ, and the lines are curve fits to

$$v_f = a\Phi^{\alpha}\,, \tag{4}$$

which show that $\alpha \approx 0.36$, and that a increases with L. The volume fractions we probe are $0.001 \lesssim \epsilon \lesssim 0.2$. The solid dots show data taken from [15] for forced drainage using a dish detergent solution, and the best fit is $\alpha \approx 0.51$. The lowest curve shows that for $L = 0.2$ cm decreasing the tube diameter from 2.5 cm to 0.6 cm decreases the front velocity by about a decade and increases α from 0.36 to 0.42.

Fig. 5 shows the measured relationship between the front width, w_f, and v_f for the set of three bubble sizes. The front width is defined as the downwards distance between the points where the profile is 80% of its maximal value and 20% of its maximal value (cf. Fig.3b). For faster waves the profile sharpens and w_f decreases. The solid lines are best-fit curves to

$$w_f = b{v_f}^{\beta} \tag{5}$$

and show that $\beta \approx -1$, and b increases with L. Data is only shown for the low fluxes. For high fluxes, or large velocities, the front width levels off, and does not continue to decrease. We speculate that this may be due to finite bubble size effects, and perhaps some subtle effects such as multiple light scattering in the foam, which depend on the foaming tube size.

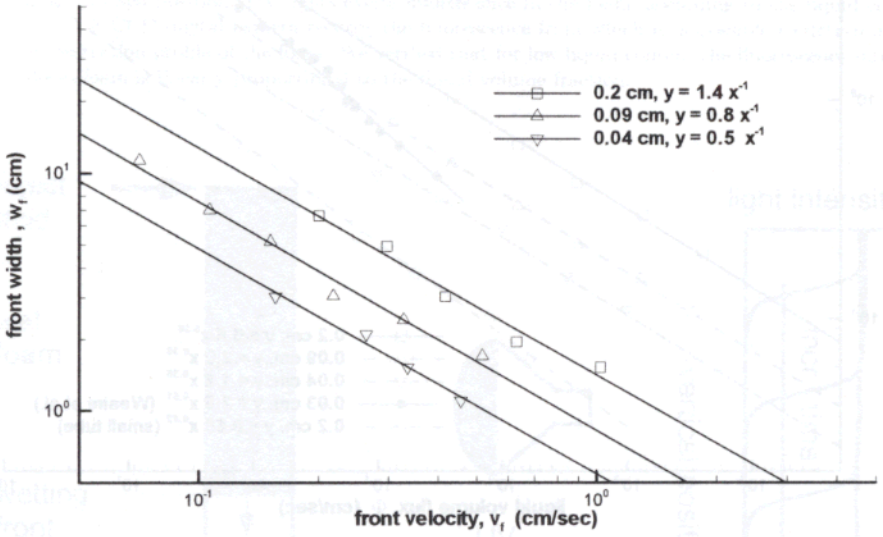

Figure 5: The dependence of the front width on the front velocity for three different bubble sizes. All three curve fits show that $w_f \propto v_f^{-1}$.

5 A General Foam Drainage Equation

The original forced drainage model [8, 16, 17] is based upon a force balance between the driving pressure gradient and the viscous damping force in the channels. In our proposed model however we rely upon an energy balance over channels *and* nodes accounting for the rate of work that drives the flow and the rate of energy loss due to viscous dissipation. We estimate that the Reynolds numbers, based upon a typical channels radius $\lesssim 10$, and neglect kinetic energy.

5.1 An Energy Argument

Consider the energy balance over a network unit, consisting of a channel with a quarter of a node attached to both ends, as the dog-bone in Fig. 1c, with liquid volume fraction $\mathcal{V}$. Balancing the rate of work per unit volume done by pressure and body forces against the viscous dissipation yields

$$\int_{\mathcal{V}} \mathbf{u} \cdot (\rho \mathbf{g} - \nabla p)\, d\mathcal{V} = -\int_{\mathcal{V}} \mu \mathbf{u} \cdot \nabla^2 \mathbf{u} d\mathcal{V}\,, \tag{6}$$

where $\rho \mathbf{g}$ is the gravitational force, p is the pressure and $\mathbf{u}$ is the liquid velocity field. The rate of work per unit volume that drives the flow in the network unit can be rewritten as

$$\overline{\mathbf{u}} \cdot \mathbf{G}\, \mathcal{V} \tag{7}$$

where $\overline{\mathbf{u}}$ is the average liquid velocity, and $\mathbf{G}$ is the macroscopic driving pressure gradient that is assumed not to vary on length scales smaller than L. The network unit volume fraction $\mathcal{V}$ consists of a node liquid volume fraction contribution $\mathcal{V}_n \approx \delta_n r^3$ and channel liquid volume fraction contribution $\mathcal{V}_c \approx \delta_c r^2 L$ (cf. (1)). Removing length and velocity scales from inside the dissipation integral yields

$$\mu\overline{u}^2\delta_n r\int_{\mathcal{V}_n/\delta_n r^3}\frac{\mathbf{u}}{\overline{u}}\cdot r^2\nabla^2\frac{\mathbf{u}}{\overline{u}}\frac{d\mathcal{V}}{\delta_n r^3}+\mu\overline{u}^2\delta_\epsilon L\int_{\mathcal{V}_c/\delta_\epsilon r^2 L}\frac{\mathbf{u}}{\overline{u}}\cdot r^2{\nabla_\perp}^2\frac{\mathbf{u}}{\overline{u}}\frac{d\mathcal{V}}{\delta_\epsilon r^2 L}+$$
$$\mu\overline{u}^2\frac{\delta_\epsilon r^2}{L}\int_{\mathcal{V}_c/\delta_\epsilon r^2 L}\frac{\mathbf{u}}{\overline{u}}\cdot L^2{\nabla_\parallel}^2\frac{\mathbf{u}}{\overline{u}}\frac{d\mathcal{V}}{\delta_\epsilon r^2 L} \tag{8}$$

where $\nabla^2_\parallel$ is the longitudinal component of the Laplacian along the channel with length scale L^{-2}, and $\nabla^2_\perp$ is the transverse component of the Laplacian with length scale r^{-2}. The first integral is the viscous dissipative work of the flow in the node regions, the second is the transverse dissipative work in the channel, and the last integral is longitudinal (extensional and compressional) dissipative work in the channel.

Equating the rates of driving with damping work ((7) and (8)) for a channel, along with some algebra yields

$$\mathbf{G}\cdot\bar{\mathbf{u}}\approx\mu\overline{\mathbf{u}}\left(\frac{\delta_n r}{\delta_\epsilon r^2 L}\int_{\tilde{\mathcal{V}}_n}\tilde{\mathbf{u}}\cdot\tilde{\nabla}^2\tilde{\mathbf{u}}d\tilde{\mathcal{V}}+\frac{\delta_\epsilon L}{\delta_\epsilon r^2 L}\int_{\tilde{\mathcal{V}}_c}\tilde{\mathbf{u}}\cdot\tilde{\nabla}^2_\perp\tilde{\mathbf{u}}d\tilde{\mathcal{V}}+\frac{\delta_\epsilon r^2}{\delta_\epsilon r^2 L^2}\int_{\tilde{\mathcal{V}}_c}\tilde{\mathbf{u}}\cdot\tilde{\nabla}^2_\parallel\tilde{\mathbf{u}}d\tilde{\mathcal{V}}\right)\,, \tag{9}$$

where $\tilde{}$ denotes dimensionless quantities, and $\bar{\mathbf{G}}$, $\bar{\mathbf{u}}$, respectively denote the unit vector in the direction of the pressure gradient, flow in the dog-bone network unit. We approximated $\mathcal{V}$ in (7) by $\mathcal{V}_c\approx\delta_\epsilon r^2 L$, in keeping with the approximations that lead to (2).

As the foam is composed of many such interconnected network units oriented in all different directions with flows along the direction of the channel, the average liquid velocity of a region of foam, $\mathbf{v}=<\overline{\mathbf{u}}>$, is given by

$$\frac{\mathbf{G}}{3}\approx\frac{\mu\mathbf{v}\delta_n}{\delta_\epsilon r L}\int_{\tilde{\mathcal{V}}_n}\tilde{\mathbf{u}}\cdot\tilde{\nabla}^2\tilde{\mathbf{u}}d\tilde{\mathcal{V}}+\frac{\mu\mathbf{v}}{r^2}\int_{\tilde{\mathcal{V}}_c}\tilde{\mathbf{u}}\cdot\tilde{\nabla}^2_\perp\tilde{\mathbf{u}}d\tilde{\mathcal{V}}+\frac{\mu\mathbf{v}}{L^2}\int_{\tilde{\mathcal{V}}_c}\tilde{\mathbf{u}}\cdot\tilde{\nabla}^2_\parallel\tilde{\mathbf{u}}d\tilde{\mathcal{V}}\,. \tag{10}$$

The factor of 3 is introduced from averaging over all channel orientations, because $<\mathbf{G}\cdot\bar{\mathbf{u}}>=\mathbf{G}/3$. The permeability of the foam (cf. (3)) then is

$$k=\left(\frac{3\delta_n}{\delta_\epsilon r L}\mathcal{I}_n+\frac{3}{r^2}\mathcal{I}_{c\,\perp}+\frac{3}{L^2}\mathcal{I}_{c\,\parallel}\right)^{-1}\approx\left(\frac{3\delta_n\delta_\epsilon^{1/2}}{L^2\epsilon^{1/2}}\mathcal{I}_n+\frac{3\delta_\epsilon}{L^2\epsilon}\mathcal{I}_{c\,\perp}+\frac{3}{L^2}\mathcal{I}_{c\,\parallel}\right)^{-1} \tag{11}$$

where $\mathcal{I}_n$, $\mathcal{I}_{c\,\perp}$ and $\mathcal{I}_{c\,\parallel}$ are the corresponding dimensionless dissipative work integrals of the dimensionless flow field $\tilde{\mathbf{u}}$. The second equality of (11) follows from (2). Calculation of these dimensionless integrals in general is quite difficult, and beyond the scope of this work, except for the simple case of no-slip channel walls.

To derive a foam drainage equation, which describes the dynamics of $\epsilon(\mathbf{x},t)$, we must relate the pressure gradient in $\mathbf{G}$ to ϵ and the surface tension. The Young-Laplace equation relates the curvature to the pressure drop across an interface

$$p=p_{\mathbf{gas}}-\gamma/r\,, \tag{12}$$

where γ is the surface tension. It is standard practice to assume that all the bubbles have the same pressure and volume, because the weight of the foam is small and compression due to gravity is negligible [9]. The driving force can be rewritten as

$$\mathbf{G}=\rho\mathbf{g}+\nabla(\gamma/r)\approx\rho\mathbf{g}+\frac{\gamma\sqrt{\delta_\epsilon}}{L}\nabla\epsilon^{-1/2}\,, \tag{13}$$

using (2). The general foam drainage equation is obtained from a conservation of mass statement,

$$\frac{\partial\epsilon}{\partial t}+\nabla\cdot(\epsilon\mathbf{v})=0\,, \tag{14}$$

which relates the change of flux through the foam to the change of liquid volume fraction. Solving for $\mathbf{v}$ from (3) and (13) gives the generalized foam drainage equation

$$\mu\frac{\partial\epsilon}{\partial t}+\rho\mathbf{g}\cdot\nabla(k\epsilon)+\frac{\gamma\sqrt{\delta_\epsilon}}{L}\nabla\cdot\left(k\epsilon\nabla\epsilon^{-1/2}\right)=0 \tag{15}$$

in terms of the permeability k given by (11).

5.2 Boundary Conditions

The original foam drainage equation [16] is based upon a no-slip (i.e. zero-velocity) boundary condition at the liquid/gas interface. The flow in the channel is Poiseuille-like, so that $\mathcal{I}_{c\perp} \approx 310$ [8]. The second term of (11) makes the dominant contribution to k because $r \ll L$. The liquid velocity then is

$$\mathbf{v}_{\text{no slip}} \approx r^2(\rho\mathbf{g} + \gamma\nabla r^{-1})/930\mu \; . \tag{16}$$

There are two arguments to justify the no-slip boundary condition. Generally it is believed that the faces of the bubbles contain very little liquid, and that there is essentially no flow in the faces. Channels and nodes are between the faces, and the bulk liquid will induce a shear on the surface that causes a surface flow. If the surface viscosity is large, then the surface flow is low, and the channel boundaries can essentially be considered rigid. Kraynik [6] proposed that for large surface viscosities, $\mu_s \gtrsim 10r\mu$, the surface velocity will be much less than the average flow velocity through the channel, and the channel essentially is rigid. A second argument for a no-slip interface is that the liquid flow through the channels will shear surfactants off the top portion of the channel surface and push them towards the bottom of the channel. If the diffusion times for surfactants in the bulk to replenish the surfaces are large, then a surfactant concentration gradient in the direction of the downwards flow is created. This sets up a surface stress that will oppose the further downwards flow of the surface, and so reduce the surface velocity.

The other limit to consider is that there are only very small surface stresses, because the surface viscosity is low and there are negligible concentration gradients in surfactants along the surface. We remind the reader that the injected liquid is the same soap solution used to generate the foam. The surface viscosity is highly dependent on the surfactant, and is known to vary over at least four orders of magnitude [18]. If the surfactant molecules are mobile enough and can quickly adsorb and desorb from the surface on the time scales of the flow, then the surfactant concentration gradient should be small. The flow in the channels would then be plug-like with some degree of extension/compression towards the top/bottom ends of the channel where the cross-sections become larger (see Fig. 1c). Thus $\mathcal{I}_{c\perp}$ is small. However in the nodes there will be dissipation due to the merging, mixing and bending of the flow (see Fig. 1b). The first term of (11) will dominate, (the third term is negligible because $L \gg r$) and the liquid velocity becomes

$$\mathbf{v}_{\text{no stress}} = \delta_\epsilon r L(\rho\mathbf{g} + \gamma\nabla r^{-1})/3\delta_n\mathcal{I}_n\mu \; . \tag{17}$$

We compare the two models ((16) and (17), i.e., no-slip and no-stress respectively) with experimental results below.

6 Forced Drainage

In forced drainage, the dependence of the front velocity on the liquid flux is measured. Everywhere in the forced drainage wave the average liquid velocity must be the same, because otherwise the wave would lose its shape as it propagates down the foam, i.e. either the front would separate from the main body, or there would be a pile-up at the front. The volumetric liquid flux equals the product of the liquid volume fraction and the velocity,

$$\mathbf{\Phi} = \epsilon\mathbf{v} = \epsilon k\mathbf{G}/\mu \; . \tag{18}$$

In the main body of the forced drainage wave all the bubbles have the same curvature, $r = r_{\max}$, and the flow is entirely driven by gravity. Using the no-slip boundary condition, (16) and (2) give

$$\Phi \approx \frac{930\delta_\epsilon\mu(v_{\text{no slip}})^2}{\rho g L^2} \Rightarrow v_{\text{no slip}} \propto \Phi^{1/2} \; , \tag{19}$$

which does not agree well with our measurements $v_f \propto \Phi^{0.36}$. Similar experiments using dish detergent and water show a different behavior, $v_f \propto \Phi^{1/2}$ [15], but the measurements extend down to only $\epsilon \approx 0.05$, which is still a fairly wet foam.

In contrast, the no-stress boundary condition (17) yields

$$\Phi \approx \left(\frac{3\delta_n\mathcal{I}_n\mu}{\delta_\epsilon^{1/2}\rho g L^2}\right)^2 (v_{\text{no stress}})^3 \Rightarrow v_{\text{no stress}} \propto \Phi^{1/3} \; , \tag{20}$$

which agrees well with our experimental observations. One plausible explanation for the somewhat larger measured exponents (i.e. $v_f \propto \Phi^{0.36}$ rather than $v_f \propto \Phi^{1/3}$) is that there may be some dissipation in the channels, i.e. the second and third terms of (8) may contribute and decrease the permeability slightly. Both boundary conditions predict an increase in front velocity with bubble size, which is also in qualitative agreement with the data (Fig. 4). We hesitate to make a more quantitative comparison because of the polydispersity of the bubbles, which we estimate to be about 30%.

We now discuss the front of the forced drainage wave. From (16) and $v = v_f$ everywhere in the forced drainage wave, Darcy's equation (3) is

$$\rho g + \gamma \frac{\partial}{\partial z} r^{-1} = \frac{930 \mu v_{\text{no slip}}}{r^2} \tag{21}$$

for the no-slip interface. (We choose the positive z in the direction of $\mathbf{g}$.) Likewise for the no-stress interface using (17) Darcy's equation is

$$\rho g + \gamma \frac{\partial}{\partial z} r^{-1} = \frac{3 \delta_n \mathcal{I}_n \mu v_{\text{no stress}}}{\delta_\epsilon r L} \; . \tag{22}$$

The solutions to these ordinary differential equations determine the shape of the forced drainage wave profile. Equation (21) with the no-slip interface boundary condition has the solution

$$r_{\text{no slip}}(z) = \left(\frac{930 \mu v_{\text{no slip}}}{\rho g} \right)^{1/2} \tanh \left(\frac{\sqrt{930 \rho g \mu v_{\text{no slip}}}}{\gamma} (z - z_0) \right) \; , \tag{23}$$

where z_0 sets the instantaneous position of the front. The no-slip prediction of the front profile fails on two accounts. First, the measured front width scales with $w_f \propto 1/v_f$ (see Fig. 5), whereas (23) predicts $w_f \propto 1/\sqrt{v_f}$. Second, the front width is independent of L, whereas we observe a clear increase in the front width with L.

The solution to (22) for the no-stress boundary condition gives

$$r_{\text{no stress}}(z) = \frac{3 \mu \mathcal{I}_n v_{\text{no stress}}}{\rho g L} \Bigg/ \left(1 + \exp \left(\frac{3 \mu \mathcal{I}_n v_{\text{no stress}}}{\gamma L} (z - z_0) \right) \right) \; . \tag{24}$$

This solution shows good agreement with the experimental measurements for both $w_f \propto v_f^{-1}$ and the increase of w_f with L, although we again hesitate to make direct comparisons because of the polydispersity of the bubble size. For a more quantitative analysis we refer the reader to [7].

7 Conclusions

We have developed a new method for measuring the liquid volume fraction of foams, which is based upon the use of fluorescence. It is possible to obtain data spanning many decades of liquid volume flux using this technique, and we observe remarkably good power-law behavior for forced drainage, especially when considering how complicated and disordered the system is.

We have presented an alternative derivation of a more general foam drainage equation which takes into account the role of nodes as well as channels for the viscous damping. We discuss two limiting cases of this equation: a no-slip interface, which is the assumption of the original foam drainage equation, and a no-stress (freely slipping) interface. The former agrees well with experimental results from many publications by Weaire et al. [9, 15, 17]. The latter agrees very well with our measurements of both the front velocity and front width of the forced drainage wave, whereas the former fails on both accounts.

Our measurements of forced drainage for foam in a narrow foaming tube show that wall effects change the power-law behavior. For the front velocity, we find an exponent between the exponent of the no-slip interface ($\alpha = 1/2$) and the zero-stress interface model ($\alpha = 1/3$) (see Fig. 4). This result fits nicely into the picture of a more general foam drainage equation, because in the narrow tube geometry a substantial amount of the flow is in channels touching the walls, where of course there is a no-slip condition. This will increase the relative importance of channel dissipation in (8), and increase the effective exponent from 1/3 towards 1/2.

In conclusion, we propose a new general foam drainage equation, and find that a no-stress liquid/gas interfacial boundary condition gives good agreement with our experiments of an aqueous foam made with water and a common dish detergent.

8 Acknowledgments

We thank the organizers of the Leuven '99 workshop "New Directions in Foam Research, Including Microgravity" for their kind invitation. A. Kraynik was extremely helpful with useful ideas and his expertise with the Surface Evlover program. G. McKinley kindly provided us with advice and fluorescein salt. We also owe thanks to A. G. Evans for his guidance and support through the MURI project on Ultralight Materials.

References

[1] J. J. Bikerman, *Foams* (Springer, New York, 1973).

[2] *Foams*, edited by R. K. Prud'homme and S. A. Khan (Marcel Dekker, New York, 1996).

[3] L. J. Gibson and M. F. Ashby, *Cellular Solids* (Cambridge University Press, Cambridge, 1997).

[4] A. G. Evans, J. W. Hutchinson, and M. F. Ashby, Curr. Opin. Solid St. M. **3**, 288 (1998).

[5] D. Desai and R. Kumar, Chem. Eng. Sci. **37**, 1361 (1982).

[6] A. M. Kraynik, Sandia National Laboratories, report No. 83-0844 (1983).

[7] S. A. Koehler, S. Hilgenfeldt and H. A. Stone, Phys. Rev. Lett., (accpeted April 4, 1999).

[8] R. A. Leonard and R. Lemlich, AIChE J. **11**, 18 (1965).

[9] D. Weaire, S. Hutzler, G. Verbist, and E. Peters, Adv. Chem. Phys. **102**, 315 (1997).

[10] A. Bhakta and E. Ruckenstein, Adv. Colloid Interface Sci. **70**, 1 (1997).

[11] H. M. Princen, Langmuir **2**, 519 (1986).

[12] Univ. Minnesota Geometry Center, Surface Evolver Version 2.10c; http://www.geom.umn.edu, 1998.

[13] A. A. Zick and G. M. Homsy, J. Fluid Mech. **115**, 13 (1982);

[14] R. E. Larson and J. J. L. Higdon, Phys. Fluids A **1**, 38 (1989).

[15] D. Weaire, N. Pittet, and S. Hutzler, Phys. Rev. Lett. **71**, 2670 (1993).

[16] I. I. Goldfarb, K. B. Kann, and I. R. Shreiber, Fluid Dynamics **23**, 244 (1988).

[17] G. Verbist, D. Weaire, and A. Kraynik, J. Phys. Condens. Matter **8**, 3715 (1996).

[18] N. F. Djabbarah, D. O. Shah, and D. T. Wasan, Colloid Polym. Sci. **256**, 1002 (1978).